Bernat-Quesada, F.; Vallés-García, C.; Montero-Lanzuela, E.; López-Francés, A.; Ferrer Ribera, RB.; Baldovi, HG.; Navalón Oltra, S. (2021). Hybrid sp2/sp3 nanodiamonds as heterogeneous metal-free ozonation catalysts in water. Applied Catalysis B Environmental. 299:1-11. https://doi.org/10.1016/j.apcatb.2021.120673

Hybrid sp^2/sp^3 nanodiamonds as heterogeneous metal-free ozonation catalysts in water

Francisco Bernat-Quesada,[1,a] Cristina Vallés-García,[1,a] Eva Montero-Lanzuela,[1] Antón López-Francés, [1] Belén Ferrer,[1] Herme G. Baldoví,[1,*] Sergio Navalón[1,*]

[1] Departamento de Química, Universitat Politècnica de València, Camino de Vera s/n, Valencia 46022, Spain

Emails: hergarba@cam.upv.es, sernaol@doctor.upv.es

Abstract

There is a growing interest from academia and industry in metal-free heterogeneous catalysts as an alternative to current non-sustainable transition metal catalysts. Herein we report a comprehensive study on the development of hybrid nanodiamonds with a diamond core and defective graphitic shells with different sp^2/sp^3 ratios as metal-free ozonation catalysts. A volcano-type trend relationship between the catalytic activities with respect to the sp^2/sp^3 ratio was found. The most active nanodiamond pyrolysed at 1100 ºC for 1 h exhibits a unique sp^2/sp^3 configuration together with an optimum amount of oxygen and nitrogen functional groups. O_3 is catalytically transformed into hydroperoxyl radicals and $^1O_2$ species. The catalytic activity of the spent hybrid nanodiamonds can be recovered by a simple annealing in an inert atmosphere that reconstitutes the defective sp^2/sp^3 hybrid nanodiamond. This study exemplifies the possibility of tailoring the physico-chemical properties of commercial nanodiamonds for the development of active metal-free ozonation catalysts.

Keywords: commercial nanodiamonds; defective core-shell sp^2/sp^3 structure; metal-free catalyst; ozonation; aqueous pollutant degradation

[a] Both are considered as first authors

1. Introduction

The development of metal-free heterogeneous catalysts is an area of great interest for academia and industry [1-9]. The ultimate goal of carbocatalysis is the replacement of transition metal catalysts by sustainable and cost-effective metal-free carbonaceous materials [10-12]. A clear example of sustainability in this area has been the use of activated carbons obtained from biomass as carbocatalysts [13, 14]. The discovery of new carbon allotropes such as nanodiamonds, carbon nanotubes or graphenes, and related carbon materials has expanded the field [15]. Currently, one of the challenges in carbocatalysis is the development of catalytically efficient carbons with atomically precise active sites and specific physico-chemical and electronic properties [16]. The reader is referred to a series of reviews dealing with the development of carbon-based materials such as graphenes,[16-20] carbon nanotubes, nanodiamonds [21-24], carbon dots [25], and other carbonaceous materials such as metal-free catalysts [1, 3, 5, 7].

Since the preparation of nanodiamonds (NDs) at an industrial scale (Tons) by the detonation method there is an increasing interest in their use for several applications including heterogeneous catalysis [21]. In the field of carbocatalysis, partially graphitized nanodiamonds have found applications as metal-free heterogeneous catalysts in some reactions used in petrochemistry, fine chemicals, and environmental remediation [21]. It is generally observed that commercial NDs annealed at temperatures of between ~700 and 1300 ºC in an inert atmosphere reveal a hybrid structure with a diamond core and graphitic shells that contain some oxygen functional groups or carbon vacancies as defects [21, 26, 27]. Annealing at higher temperatures results in the formation of onion-like carbons exclusively constituted by sp^2 carbons. As one representative example in the area of petrochemistry, Su and co-workers used partially graphitized NDs as

carbocatalysts for the dehydrogenation of hydrocarbons such as ethylbenzene[28] and propane[29].

In the area of environmental applications, sp^2/sp^3 hybrid NDs have found applications as metal-free catalysts in advanced oxidation processes (AOP). For example, Shaobin and co-workers have reported the possibility of using these hybrid NDs as active carbocatalysts for peroxymonosulfate [30-32] activation and aqueous phase pollutant degradation [1]. In the area of AOPs there is increasing interest in the development of heterogeneous catalytic ozonation processes due to their relatively easy implementation at an industrial scale [33]. The aim of catalytic ozonation is to increase the reactivity of molecular O_3 towards organic or inorganic compounds through the formation of reactive oxygen species (ROS) such as hydroxyl, hydroperoxyl, superoxide radicals, and $^1O_2$ [33]. Homogeneous (i.e. Co(II), Fe(II), Mn(II)) and heterogeneous transition metal catalysts (i.e. MnO_2, TiO_2, Al_2O_3, CeO_2) have been reported as active ozonation catalysts [33-35]. Importantly, several studies have shown the possibility of using carbon-based materials such as activate carbons [36-42], carbon nanofibers [43], carbon nanotubes [40, 44], graphene and related materials [45, 46] as metal-free catalysts for heterogeneous catalytic ozonation [47]. Commonly, oxalic acid is used as organic probe molecule to determine the extent of catalytic ozonation in water, since molecular O_3 itself in the absence of catalyst can barely degrade it under real water treatment conditions [45, 48, 49]. Thus, the observation of oxalic acid degradation during ozonation can serve to assess the catalytic activity, promoting the decomposition of molecular O_3 towards those ROS able to degrade oxalic acid. Other studies have employed the catalytic ozonation for the degradation of a large variety of organic compounds, including pharmaceuticals, personal care products and other chemicals such as bisphenol A that can be present as pollutants in waters [50].

With these precedents we report the development of hybrid and defective sp^2/sp^3 NDs as heterogeneous metal-free catalysts for O_3 activation and oxalic acid degradation as a model pollutant in water. The characterisation data and catalytic activity reveal the importance of an optimized sp^2/sp^3 structure containing oxygen and nitrogen functional groups on NDs to achieve an excellent level of activity. We are confident that this study will help in the development of nanocarbons with a surface functionalisation that is adequate for acting as active sites for oxidation reactions.

2. Experimental section

2.1. Materials and methods

Diamond nanopowder (ref: 1321JGY, >98 % purity) was supplied by Nanostructured & amorphous materials, Inc. Dimethyl sulfoxide (DMSO, >99.5%), *tert*-butanol (> 99%), NaN_3 (S2002, >99.5 %), 5,5-dimethyl-1-pyrroline N-oxide (DMPO), and 2,2,6,6-tetramethylpiperidine (TEMP) were supplied by Merck. All other chemicals and solvents employed in this study were analytical or HPLC grade and they were also provided by Merck.

Hybrid sp^2/sp^3 nanodiamond preparation. Commercial diamond nanopowder (Commercial ND; 200 mg) was placed in a tubular oven under argon atmosphere and heated at the corresponding temperatures (700, 900, 1100, 1200 ºC) at 5 ºC/min for 1 or 4 h. The resulting samples were washed ethanol and water and finally dried at 100 °C for at least 12 h. The samples were labelled as a function of the temperature and annealing time as follows: ND-700, ND-900, ND-1000, ND-1100, ND-1100-4h, ND-1200.

Reactivation of used ND in catalysis. After the reaction, the partially deactivated and most active ND-1100 sample (ND-1100-U, where U means used) was collected from the

aqueous solution by filtration through a 0.45 μm filter and washed with Milli-Q water (500 mL). Then, the ND-1100-U sample was dried in an oven at 100 ºC for at least 12 h. Finally, the ND-1100-U was reactivated in a tubular oven under argon atmosphere by heating the sample at 1100 ºC at 5 ºC/min for 1 h. The resulting sample was labelled as ND-1100-1U-react.

2.2. Characterization

Powder X-ray diffractograms (PXRD) were performed in a Philips XPert diffractometer (40 kV and 45 mA) using Ni filtered Cu Kα radiation. UV-Raman spectra were collected at room temperature upon 315 nm laser excitation using a Renishaw In Via Raman spectrophotometer equipped with a CCD detector. X-ray photoelectron spectroscopy (XPS) of measurements were recorded with a SPECS spectrometer with an MCD-9 detector using a monochromatic Al (Kα = 1486.6 eV) X-ray source. The C 1s peak at 284.4 eV was employed as reference. High resolution transmission electron microscopy (TEM) images of nanodiamonds samples were acquired using a JEOL JEM-2100F instrument operating at 200 kW. Isothermal N_2 adsorption measurements were carried out using an ASAP 2010 Micromeritics station.

2.3. Catalytic activity

Catalytic Reactions. Catalytic ozonations were carried out as previously reported [45]. Figure S1a shows several photographs of the ozonation system employed in this study. Briefly, ozone generation was carried out using a commercially available ozone generator equipped with corona discharge technology. The generated ozone flow (140 mg_O_3/h, 570 mL/min) was introduced through a gas diffuser into the bottom of a glass reactor (250 mL; Figure S1b and S1c). The glass reactor equipped (ref. E-33978, VIDRAFOC S.A., Alboraia, Valencia, Spain) with the gas diffuser (VITRAPOR with pore size 100-160 μm,

VIDRAFOC S.A) is commercially available. The catalytic experiments were carried out introducing the oxalic acid aqueous pollutant (50 mg L^{-1}; 250 mL) together with the dispersed NDs (100 mg L^{-1}) in the glass reactor. Before introducing the ND aqueous suspension into the glass reactor the suspension was sonicated (450 W for 20 min). Figure S1d shows the ND-1100 catalyst well-suspended and floats freely in the aqueous solution of oxalic acid at pH 3 during the catalytic ozonation (140 mg_O_3/h and 570 mL/min). The course of oxalic acid degradation has been followed by analysing reaction aliquots previously filtered (Nylon filter 0.2 μm) in an ion chromatograph instrument (Metrohm) equipped with a conductivity detector. The stationary phase was a column of poly(vinyl alcohol) with quaternary ammonium groups (Metrosep A Supp 5), while the mobile phase was a basic aqueous solution (Na_2CO_3 3.2 mM / $NaHCO_3$ 1.0 mM).

The ozone concentration generated by the ozonator was determined by using the iodometry method. Briefly, the ozonated air was introduced in the glass reactor through the glass diffuser (Figure S2a). Previously, an acidified aqueous solution of KI (2 g/L; 250 mL; 0.25 mL $H_2SO_{4(c)}$) was introduced in the glass reactor. Thus, the generated ozone reacts with KI leading to the formation of I_2. Subsequently, the formed I_2 was titrated using an aqueous solution of sodium thiosulfate (0.01 N). Control experiments showed that no ozone escapes from the reactor since analysis of the gas exiting reactor 1 in a second connected vessel with acid aqueous KI solution shows the absence of (Figure S2a). A series of analogous preliminary experiments determine the percentage of generated ozone (140 mg/h; 570 mL/min) introduced in the glass reactor 1 (Figure S2b) containing Milli-Q water, Milli-Q water with oxalic acid (50 mg/L) or Milli-Q water with oxalic acid (50 mg/L; 200 mL) and the ND-1100 catalyst (100 mg/L) that is consumed in the system by quantifying the ozone in the outlet flow. In these measurements, the gas exit of the glass reactor 1 was connected to other glass reactor 2 containing the acid KI

aqueous solution. In this way, it was estimated that about 38 % of introduced ozone to the mentioned different solutions escapes from the system. Therefore, an effective ozone flow of about 86.8 mg/h is present in the system during the ozonation experiments.

The concentration of ozone during the catalytic ozonation of oxalic acid at pH 3 in the absence and in the presence of substrate using ND-1100 was estimated by iodometry. Briefly, during the ozonations different reaction aliquots (15 mL) previously filtrated (0.45 μm Nylon filter) were titrated by iodometry.

The heterogeneity of the reaction during the catalytic ozonation using ND-1100 as metal-free catalyst was performed as follows. Once the oxalic acid conversion reached about 50 % an aliquot of the reaction system was sampled and the catalyst removed by filtration (Nylon filter 0.45 μm). Then, the aqueous reaction phase in the absence of catalyst was allowed to react with ozone under the described reaction conditions.

Selective quenching experiments were carried out as described for oxalic acid but with the addition of DMSO or *tert*-butanol as selective hydroxyl radical quenchers (20 mol % respect to oxalic acid) or in the presence of NaN_3 (20 mol % respect to oxalic acid) as selective $^1O_2$ quencher once the reaction is initiated (~20 % conversion).

EPR measurements. Liquid phase EPR measurements were carried out using DMPO or TEMP as spin trap. Briefly, an aqueous DMPO or TEMP solution (1 g/L; 25 mL) containing the ND-1100 as catalyst (5 mg) a pH 3 was introduced in the ozonator system (140 mg/h) for 30 min. EPR spectra of filtered (0.45 mm Nylon filter) and argon-purged aliquots (5 mL) were measured in a Bruker EMS spectrometer (9.803 GHz, sweep width 3489.9 G, time constant 40.95 ms, modulation frequency 100 kHz, modulation width 1 G, and microwave power 19.92 mW). Similarly, solid phase EPR measurements

were carried out using an argon-purged quartz support containing the ND samples and the spectra recorded at 100 K.

Total organic carbon (TOC) measurements of the reaction aliquot at the end of the catalytic ozonation (180 min) using ND-1100 as metal-free catalyst were carried out using a High TOC Elementar II analyzer.

3. Results and discussion

3.1. Catalyst preparation

In the first step of this study a series of defective hybrid sp^2/sp^3 nanodiamonds were prepared by submitting commercial NDs to several thermal treatments in an argon atmosphere at different temperatures and annealing. Powder XRD of commercial NDs shows the presence of characteristic diffraction patterns (111) and (220) of polycrystalline NDs (Figure 1). In addition to these diamond diffraction patterns, thermally annealed NDs also show the presence of characteristic graphitic materials (Figure 1). The appearance of a new broad band centred about 26 º for the ND samples annealed at temperatures above 1000 ºC is remarkable. This band is characteristic of the stacking of graphitic carbon atoms with hexagonal crystalline arrangements. These XRD variations agree with previous reports showing the formation of graphene layers from the external surface to the core of the NDs. In fact, the thermally annealed NDs at temperatures above 1000 ºC exhibited broadened and less intense diamond peaks than pristine ND. This observation agrees with the reduction of the diamond core and concomitant formation of graphitic shells. Therefore, the higher the annealing temperature or time, the greater the degree of graphitisation of the samples.

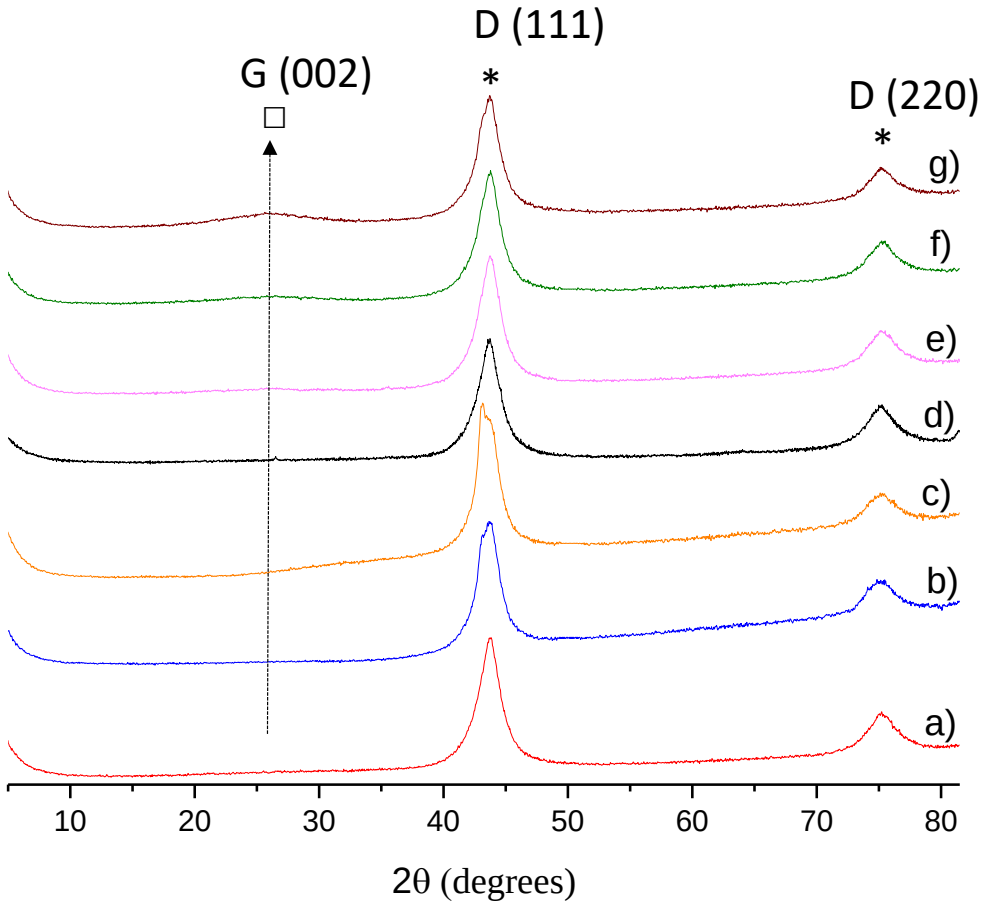

Figure 1. PXRD of commercial (a) and thermally annealed NDs in argon (b-f). Legend: a) commercial ND; b) ND-700, c) ND-900, d) ND-1000; e) ND-1100; f) ND-1100-4h; g) ND-1200.

High resolution transmission electron microscopy (HR-TEM) measurements of commercial and graphitized NDs in an argon atmosphere (Figure 2 and Figures S3-S9) confirm that high annealing temperatures or long annealing times result in the formation of core-shell structures with a large number of graphene-like layers around a diamond core. Commercial NDs (3 - 10 nm size) are characterised by a crystalline diamond core with (111) planes corresponding to an interplanar distance of about 0.21 nm that are surrounded of unstructured amorphous carbon frequently referred to as soot-matter (Figure 2a). The annealing of commercial NDs at 700 or 900 ºC for 1 h still shows the presence of a dominant diamond core with a somewhat disordered graphitic outer shell

(Figure 2b,c). When the annealing temperature is above 1000 ºC a clear transformation of the commercial ND into a core-shell hybridized sp^2/sp^3 ND with more graphitic layers is observed (Figures 2d, e). The sample annealed at 1200 ºC for 2 h exhibits the greatest graphitic appearance with the formation of highly ordered onion-like carbon (OLC) structures (Figure S8) while the core diamond domains can still be observed (Figure S9). The self-compression of the graphitic layers results in a lower plane interdistance between the internal layers (ca 0.42 nm) than the most external layers (ca 0.59 nm) (Figure S8).

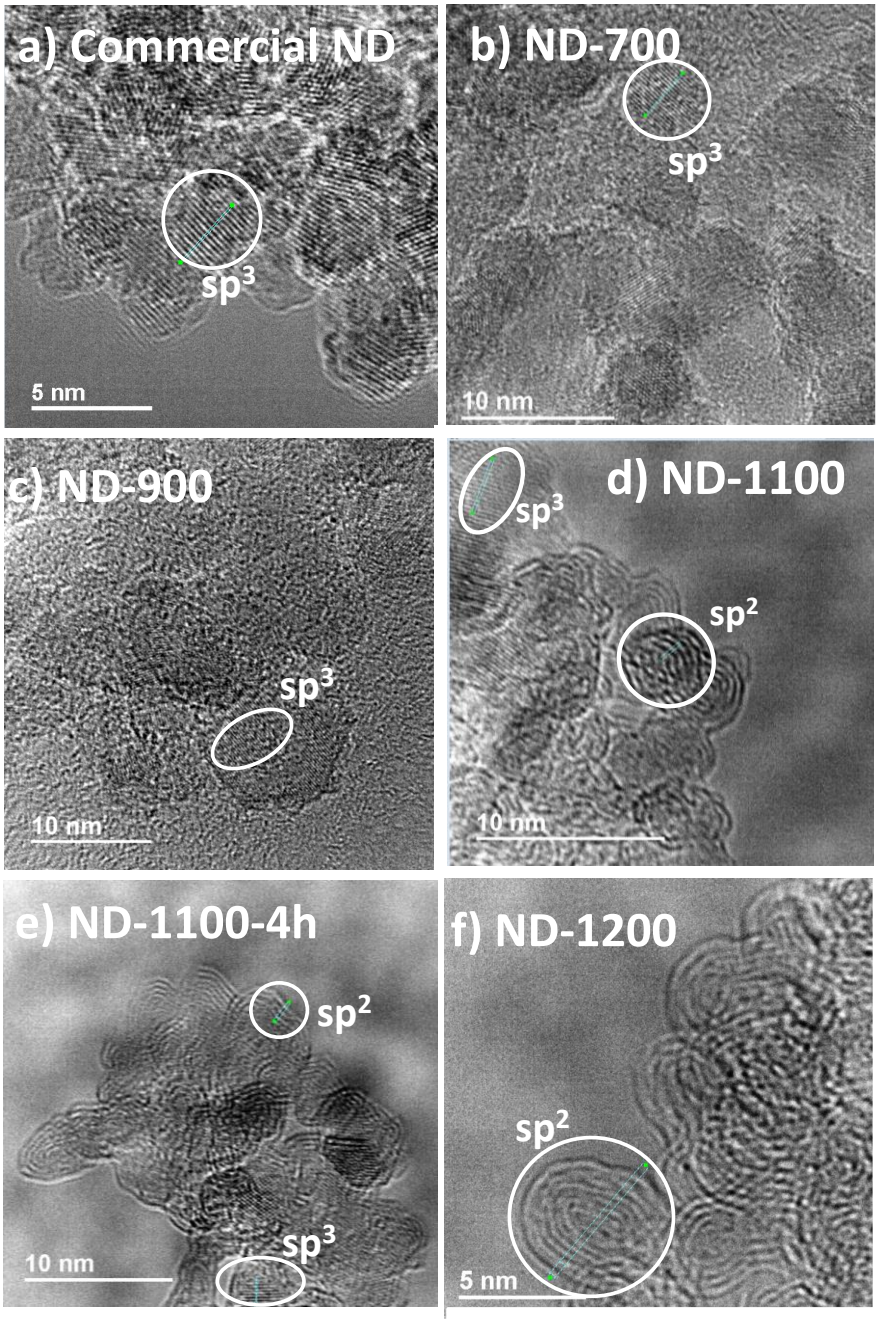

Figure 2. Photographs and HR-TEM images of commercial (a) and thermally annealed NDs in argon (b-f). Legend: a) commercial ND; b) ND-600 c) ND-700, d) ND-900; f) ND-1100; g) ND-1100-4h; h) ND-1200.

UV-Raman spectroscopy further confirmed an increase in the degree graphitisation of thermally annealed NDs along with increased annealing temperatures and times (Figures 3a and Figure S10). Figure 3a shows that increasing annealing temperatures or times results in a decrease of the diamond intensity peak at 1326 cm^{-1} together with an increase in graphitic carbon bands (namely, D band at about 1405 cm^{-1} and G-band at 1590 cm^{-1}) [51, 52]. The bands centred at about 1640 and 1720 cm^{-1} are characteristic of hydroxyl and carbonyl groups, respectively [51], and become less important with respect to the graphitic carbon bands (1405 and 1590 cm^{-1}) as the temperature or annealing time increases. A comparison of the I_D/I_G ratios of the different samples reveals that the number of defects in annealed NDs decreases as the annealing temperature or time increases. Overall, the amorphous carbon present in the commercial NDs is transformed/reconstituted during the thermally annealing process into a well-ordered nanocrystalline graphite shell and the diamond core simultaneously decreases [29]. The higher the annealing temperature and time, the fewer are the structural defects and the greater are the presence of OLC structures.

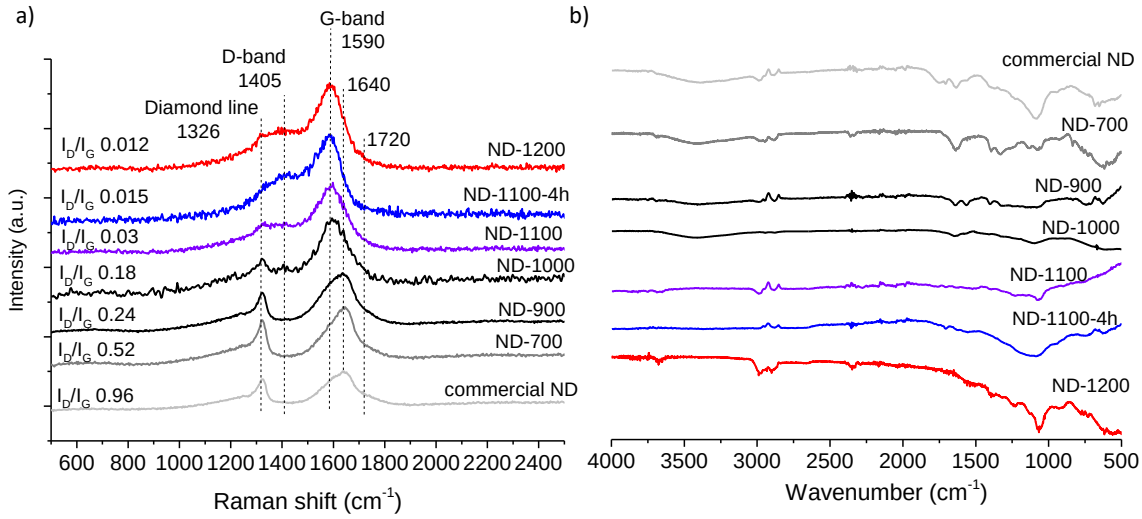

Figure 3. UV-Raman (a) and FT-IR (b) spectra of commercial ND and thermally annealed NDs in argon.

FT-IR spectroscopy has been employed to further study the changes of surface functional groups during the thermal annealing of commercial ND in an Ar atmosphere (Figure 3b). The FT-IR spectrum of commercial NDs shows the presence of several free alcohol groups (3677 and 1094 cm^{-1}) together with a broad band from 1830 till 1704 cm^{-1} that is characteristic of carbonyl groups including anhydrides, esters, lactones, cyclic ketones and carboxylic acids [29, 53]. The bands centred at 1640 and 1384 cm^{-1} can be assigned to a series of alkenes and alkanes functional groups, respectively. The broad band centred at 1080 cm^{-1} is characteristic of C-OH or C-O-C bonds. Annealing of commercial ND at 700 ºC causes the removal of the carbonyl groups centred at about 1740 cm^{-1} together with a shift down of the C-O and/or C-O-C band. Annealing at temperatures higher than 900 ºC further causes the loss of the band centred at 1640 cm^{-1} that is attributable to alkenes, together with the appearance of a broad band centred at about 1580 cm^{-1} that is characteristic of aromatic C=C bonds. This data confirms that the thermal annealing of commercial ND at increased temperatures or times results in the

graphitisation of the samples while some oxygen-functional groups – such as alcohols or ether and phenols – remain even at temperatures as high as 1200 ºC.

The degree of graphitisation of the thermally annealed commercial NDs was quantified using XPS (Figure 4 and Figures S11-S12). The higher the annealing temperature and the longer the annealing time, the higher the sp^2/sp^3 ratio (Figure 4a) together with a decrease in oxygen content (Figure 4b). The ND-1200 sample exhibits the higher sp^2/sp^3 ratio and reduced oxygen content. Similarly, XPS N1s shows that the nitrogen content of commercial ND (1.3 at%) decreases as the annealing temperature increases up to 0.9 at % (Figure S13).

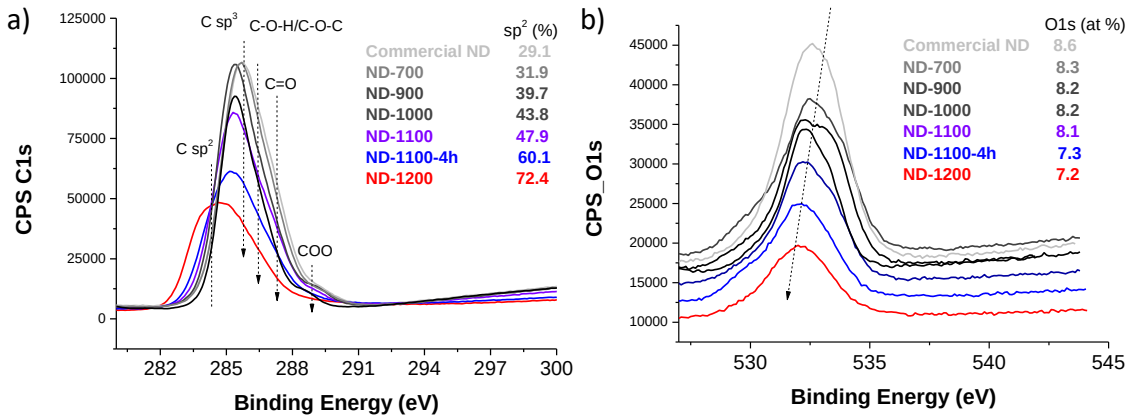

Figure 4. XPS C1s (a) and O1s (b) of commercial ND and thermally annealed NDs in argon.

In agreement with previous reports, isothermal N_2 adsorption measurements (Figure S14) of thermally annealed NDs at temperatures below 1000 ºC exhibit similar BET surface areas as the commercial ND sample (286 m^2/g) while annealing at higher temperatures shows slightly higher values (311 m^2/g) and this is attributed to the thermal expansion of stacked nanodiamonds as the temperature increases [29].

3.2. Catalytic activity

The series of graphitized ND were employed as metal-free catalysts for the ozonation of oxalic acid as a model pollutant. In agreement with previous reports on the absence of catalysts, a negligible oxalic acid degradation was observed when working at pH 3 (Figure 5a). Control experiments using the series of ND under study reveal that the adsorption of oxalic acid at pH 3 is lower than 2 wt% in all cases. Interestingly, graphitisation of commercial NDs from 600 to 1100 ºC for 1 h results in a gradual increase in catalytic activity for oxalic acid degradation at pH 3 (Figure 5a,b). In contrast, graphitisation of ND at 1200 ºC for 1 h resulted in a sample with slightly lower catalytic activity than the ND-1100 sample (Figure 5a,b). Attempts to increase the catalytic activity of the optimised ND-1100 sample by preparing an analogous sample graphitised at 1100 ºC for 4 h resulted in a sample with less activity (Figure 5a,b). Thus, the ND-1100 sample exhibits the highest catalytic activity for oxalic acid degradation. During the oxalic acid ozonation in the absence of in the presence of ND-1100 as catalyst the concentration of ozone in the liquid phase was estimated to be 0.50 ± 0.14 and 0.15 ± 0.05 mg/L, respectively. It should be noted that the catalytic activity of the ND under study does not correlate with the specific BET surface area of the materials and, therefore, other key factors should be responsible for the observed catalytic activity. From XPS it can be concluded that the sp^2/sp^3 ratio increases as the annealing temperature or time increases (Figures 4 and 5c). Interestingly, a volcano-type trend of the catalytic activity with respect to the sp^2 fraction was observed for the carbocatalytic ozonation of oxalic acid at pH 3 (Figure 5d). Figure 5d shows the catalytic activity gradually increasing together with the sp^2 fraction of the ND samples up to the ND-1100 sample. However, further graphitisation of the ND-1100-4 and ND-1200 samples resulted in a decrease in activity. This data

reflects the importance of a high proportion of sp^2 carbons, while other factors should be considered to explain the volcano-trend observed.

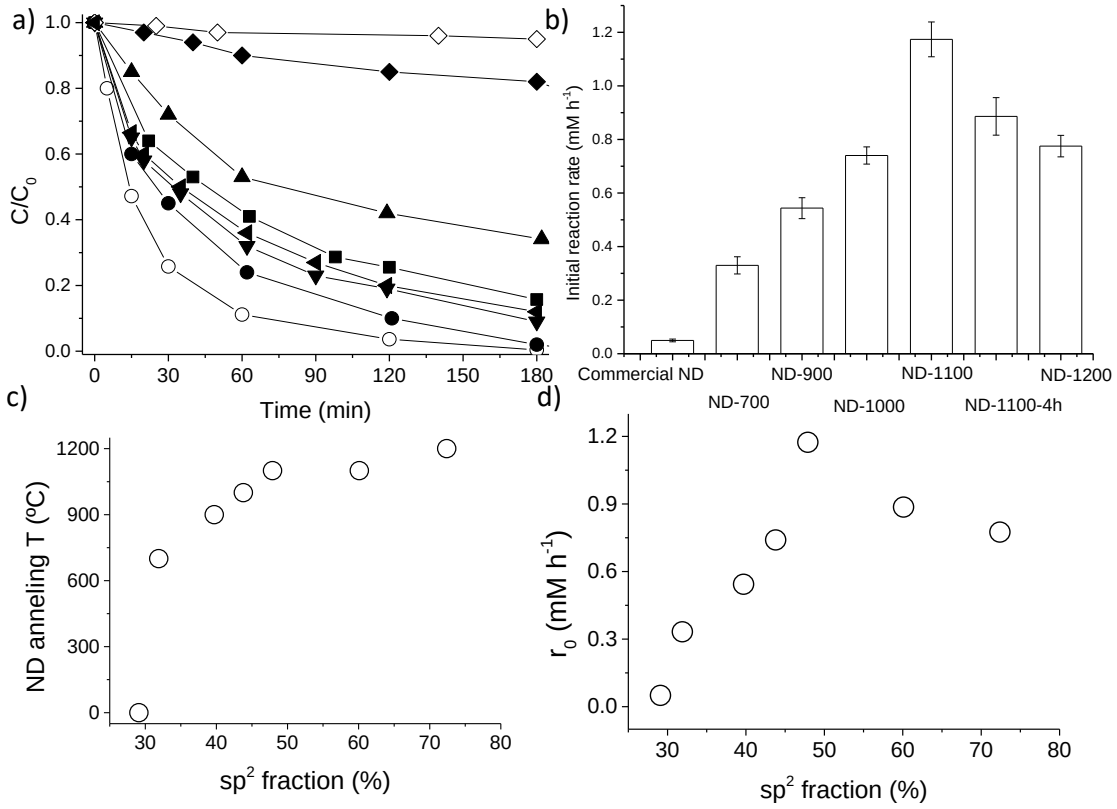

Figure 5. a) Carbocatalytic ozonation of oxalic acid at pH 3 using commercial ND and thermally annealed NDs in argon. Legend: no catalyst (◊), commercial ND (♦), ND-700 (▲), ND-900 (■), ND-1000 (◄), ND-1200 (▼),ND-1100-4h (●), ND-1100 (○). b) Initial reaction rate of oxalic acid degradation during the catalytic ozonation at pH 3 using NDs. c) ND annealing temperature versus sp2 fraction in NDs. d) Initial reaction rate of the oxalic acid degradation during the catalytic ozonation at pH 3 using NDs with different sp^2 proportions. Note: A maximum of 2 wt% of oxalic acid disappearance during the catalytic ozonation corresponds to adsorption process on hybrid NDs. Reaction conditions: Oxalic acid (50 mg/L), carbocatalyst (100 mg/L), pH 3, temperature 20 ºC, O_3 inlet to the glass reactor (140 mg/h).

In a related precedent we reported that the carbocatalytic activity of a graphite-based material can be increased by introducing hydroxyl functional groups at the edges of the graphene layers [45]. The presence of phenolic groups on the graphene sheets increases the work function of the graphite-based material and, thus, facilitates one-electron transfer mechanism leading to the simultaneous formation of semiquinone-like units and $O_3^{\cdot-}$ species. Thus, a graphite-like structure with phenolic and semiquinone-like centres is formed. These phenolic/quinone-like subunits in carbon-based materials have been proposed by several authors as redox sites catalysing various reactions including the carbocatalytic dehydrogenation of ethylbenzene [28], aerobic oxidation of cyclohexane [54], Fenton [55] and photo-Fenton [56] reactions, as well as peroxymonosulfate activation [57]. Similarly, Shaobin and co-workers proposed that the presence of sp^3 diamond cores in the sp^2/p^3 diamond nanohybrids enrich the charge density of the graphitic shells, and so favour electron transfer to PMS [30]. It should be, however, commented that as ND samples are obtained from explosive detonation and contain a residual N content, even exposed at the surface (Figure S121), similar role to oxygen can be also played in the present case of NDs by nitrogen in those substructures with aniline/imine functional groups [21].

From XPS measurements (Figure 4 and Figures S9-S10) it can be concluded that the most active samples (namely, ND-1000, ND-1100, ND-1100-4h and ND-1200) exhibit a similar proportion of oxygen-functional groups such as ketonic/quinoid, hydroxyls, and carboxylic derivatives. From XPS it can be also observed that the ND-1100 sample exhibits a somewhat higher oxygen content (8.1 at%) than ND-1100-4h (7.3 at %) or ND-1200 (7.2 at%). Similarly, the ND-1100 sample exhibits slightly higher nitrogen content (1.1 at%) than ND-1100-4h (0.9 at%) or ND-1200 (0.9 at%) (Figure S11). Considering the related commented precedents, the characterisation data of the ND

samples under study and the observed catalytic activity, we attribute the higher activity of the ND-1100 sample to a synergistic effect between a unique sp^2/sp^3 configuration and the presence of oxygen and nitrogen functional groups in the graphitic surface that benefits both the charge density and work function of the graphitic layers. The lower carbocatalytic activity of ND-1100-4h or ND-1200 samples is attributed to their higher degree of graphitisation and lower population of oxygen and nitrogen functional groups on the graphene layers that results in a lower work function than the optimized ND-1100 sample. In contrast, the ND-1000 sample with slightly higher oxygen content (8.2 at%) than the most active ND-1100 (8.1 at%) exhibits lower catalytic activity. It should be noted that the proportion of oxygen functional groups in ND-1000 and ND-1100 are very similar (Figure S10d and S10e) while both samples exhibit the same nitrogen content (1.1 at%, Figure S11). Thus, the lower content of sp^2 carbons (43.8 %) present in ND-1000 respect to ND-1100 (47.9 %) seems to be responsible for the comparatively lower catalytic activity of the former catalyst. The other samples annealed at temperatures below 1000 ºC exhibited poor activity due to their low sp^2 content and despite higher oxygen or nitrogen contents. In fact, the commercial D sample with the lowest sp^2 content and the highest oxygen and nitrogen content shows almost negligible activity.

Overall the trend in the catalytic activity of ND-x agrees with previous reports in the literature on the ozonation activity of reduced graphene oxides as metal-free catalysts [1, 46]. This study has proposed electron-rich carbonyl groups as electron donors sites to ozone [46]. In the present case, the density of these type of sites on the ND-x surface would grow with the oxygen content and with the sp^2/sp^3 ratio, determined in XPS by the growth of the C-O component and graphitic C atoms, respectively. Thus, through electron delocalization in the π system, conjugated carbonyl groups, most probably in the enolic/hydroquinone-like form, will donate electrons to O_3.

The influence of the solution pH on the resulting catalytic activity using ND-1100 was observed as catalytic activity increased as the pH values decreased (Figure 6). Control experiments using the ND-1100 sample have shown that the adsorption of oxalic acid at pH values between 3 and 9 is lower than 2 wt%. In a previous study some of us have reported that ozone stability decreases as the pH of the aqueous solution increases, and therefore, the available O_3 in solution decreases along with the pH value [45]. Other studies have shown than O_3 can decompose in basic medium to reactive oxygen species such as hydroxyl or hydroperoxyl radicals [33]. In the present study, the lower level of catalytic activity observed when using ND-1100 as the pH increases can be attributed to less ozone interacting with the catalyst for the formation of ROS.

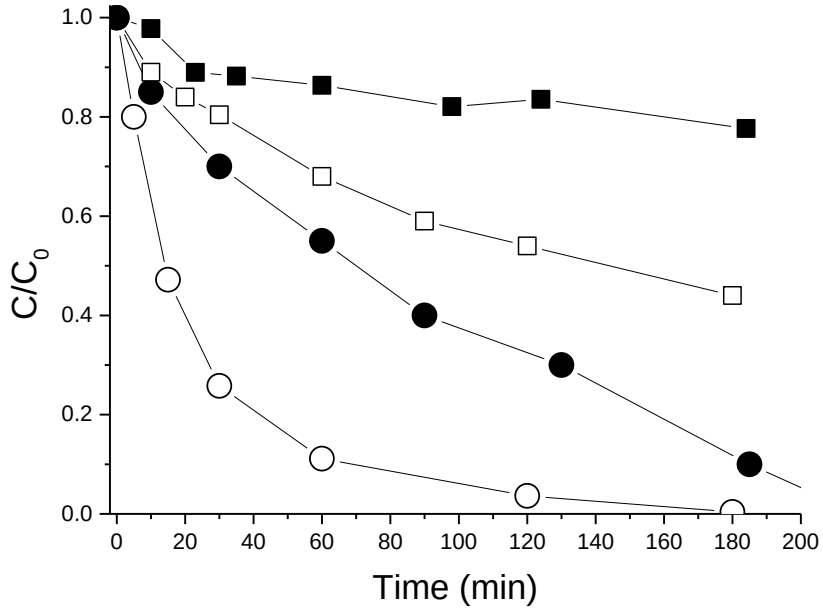

Figure 6. Carbocatalytic ozonation of oxalic acid at different initial pH values using ND-1100. Legend: pH 3 (○), pH 5 (●), pH 7 (□) and pH 9 (■). Note: A maximum of 2 wt% of oxalic acid disappearance during the catalytic ozonation corresponds to adsorption process on ND-1100. Reaction conditions: Oxalic acid (50 mg/L), carbocatalyst (100 mg/L), pH 3, temperature 20 ºC, O_3 inlet to the glass reactor (140 mg/h).

3.3. Catalyst heterogeneity and stability

The heterogeneity of the reaction was assessed by performing a filtration test. Figure 7 shows that once the reaction is initiated, if the catalyst is removed and the liquid phase can react under the same conditions, then the oxalic acid degradation stops. Thus, it can be concluded that the carbocatalytic ozonation process using ND-1100 is truly heterogeneous. Furthermore, catalyst stability of the most active ND-1100 sample was assessed by performing several reuses. As can be seen in Figure 7, the catalytic activity decreases on reuse. In a couple of precedents using reduced graphene oxide (rGO) [46] or edge-hydroxylated high surface area graphite [45] as ozonation carbocatalysts, it was reported that catalyst deactivation during the ozonation process is due to the partial oxidation of the catalysts and catalyst reactivation can be obtained by submitting the catalyst to pyrolysis treatment. With these precedents in mind, the used ND-1100 sample was submitted to an annealing treatment at 1100 ºC for 1 h. Interestingly, Figure 7 shows that this process enables recovering the catalytic activity of the fresh ND-1100 and the process can be repeated several times. Even though it is possible to recover the catalytic activity of partially spent ND-1100, from the perspective of application of hybrid ND as ozonation catalyst in water treatment would be important further increase catalyst stability. In general, the stability of nanocarbons reported as ozonation catalyst is still a far from their use for real applications [58, 59].

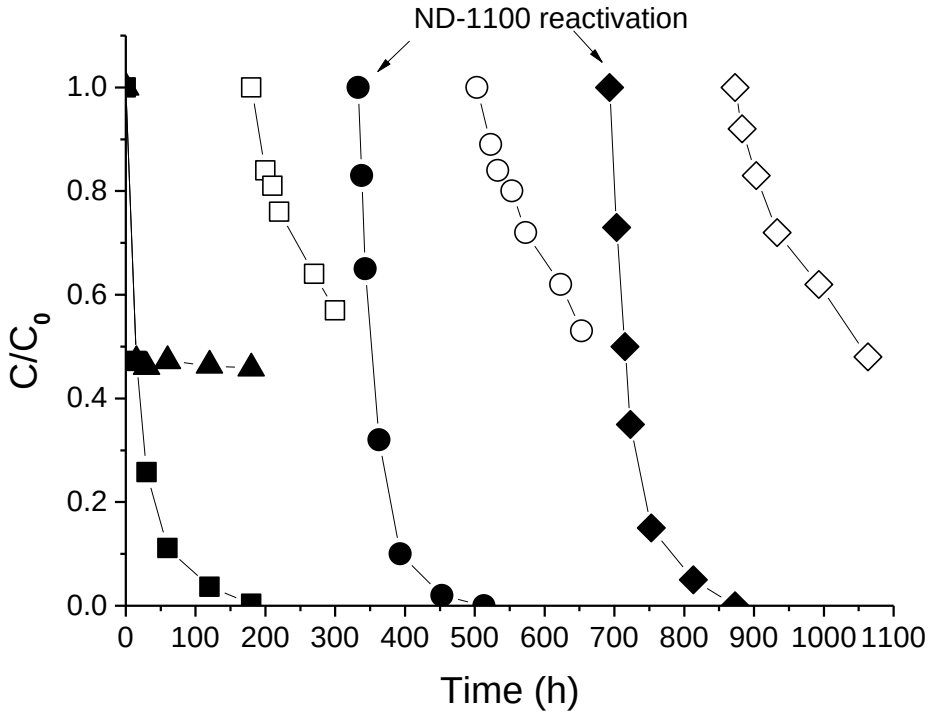

Figure 7. Reusability of the ND-1100 as a metal-free catalyst during the ozonation of oxalic acid at pH 3. Legend: 1st use (■), 2nd use (□), 3rd use after reactivation (●), 4th use (○), 5th use after reactivation (♦), 6th use (◊). Ozonation of oxalic acid after ND-1100 removal at 52% conversion (▲) during the 1st catalytic cycle (■).Note: A maximum of 2 wt% of oxalic acid disappearance during the catalytic ozonation corresponds to adsorption process on ND-1100. Reaction conditions: Oxalic acid (50 mg/L), carbocatalyst (100 mg/L), pH 3, temperature 20 ºC, O_3 inlet to the glass reactor (140 mg/h).

To obtain insights about the deactivation-activating process, the used ND-1100-1U and reactivated ND-1100-1U-react sample were characterised by PXRD (a series of spectroscopic techniques including UV-Raman, FT-IR, XPS, and EPR together with TEM measurements). PXRD of the used ND-1100-1U sample shows a decrease in the broad band centred about 26 º – which is a characteristic of the graphitic layers present in the fresh ND-1100 (Figure 8a). Interestingly, the reactivated ND-1100-1U-react sample again

shows this graphitic band in the fresh carbocatalyst (Figure 8a). In good agreement with these observations, TEM measurements reveal that the used ND-1100-1U sample is characterised by fewer graphitic layers and a correspondingly higher number of diamond planes than the fresh ND-1100 sample (Figure 8a,b and Figure S15). Moreover, thermal annealing of the used ND-1100-1U sample again enables the re-graphitisation of this sample (Figure 8c and Figure S16).

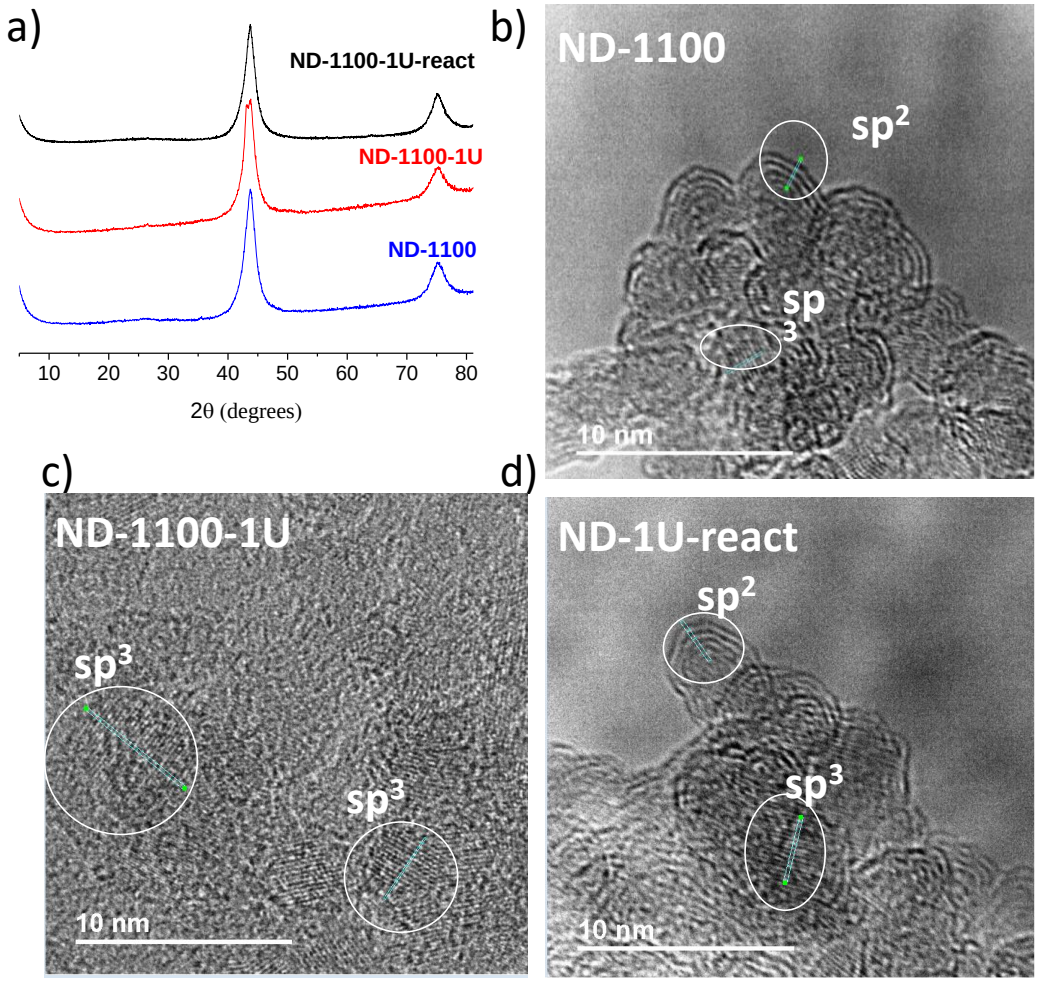

Figure 8. PXRD (a) and TEM images of ND-1100 (b), ND-1100-1U (c) and ND-1100-1U-react (d).

UV-Raman, FT-IR, and XPS spectroscopies further confirmed the changes observed by PXRD and TEM measurements. The Raman spectra of the ND-1100-1U sample is characterised by a diamond peak intensity at 1326 cm^{-1} higher than that of fresh

ND-1100 – together with a decrease in the graphitic D and G-bands (Figure 9a and Figure S17). Furthermore, the partial oxidation of the ND-1100-1U sample is characterised by an increase of the characteristic bands of hydroxyl and carbonyl groups appearing at 1640 and 1720 cm^{-1}, respectively (Figure 9a and Figure S17). In contrast, the ND-1100-1U-react sample recovers the UV-Raman features of the fresh ND-1100 sample characterised by a graphitised diamond outer part with a small proportion of oxygen-functional groups (Figure 9a and Figure S17). Moreover, the increased I_D/I_G ratio of the ND-1100-1U sample in comparison with the fresh ND-1100, together with the recovery of the I_D/I_G ratio of the ND-1100-1U-react in comparison with the fresh sample, agree with the partial oxidation and reconstitution of the ND samples (Figure 9a). Moreover, the FT-IR spectrum of the ND-1100-1U sample reveals an increase in the hydroxyl, carbonyl, and carboxylic functional groups in comparison with the fresh ND-1100 sample – while the ND-1100-1U-react sample recovers the characteristic FT-IR bands of the fresh ND-1100 sample (Figure 9b). Analogously, comparison of the XPS spectra of the fresh ND-1100 sample with the ND-1100-1U sample shows a shift in the binding energies of both C1s and O1s spectra to higher values attributable to the partial oxidation of the ND-1100 surface (Figure 9c,d and Figure S18). A more intense O1s spectrum for the used ND-1100 sample in comparison with the fresh sample further confirms the oxidation of the ND-1100 surface after use (Figure 9d). Quantitative XPS analyses of the sp^2 carbon fractions as well as oxygen and nitrogen content present in the ND-1100 samples confirm that the used ND-1100 sample becomes oxidised and can be reactivated after pyrolysis at 1100 ºC for 1 h (Figure 9c-e).

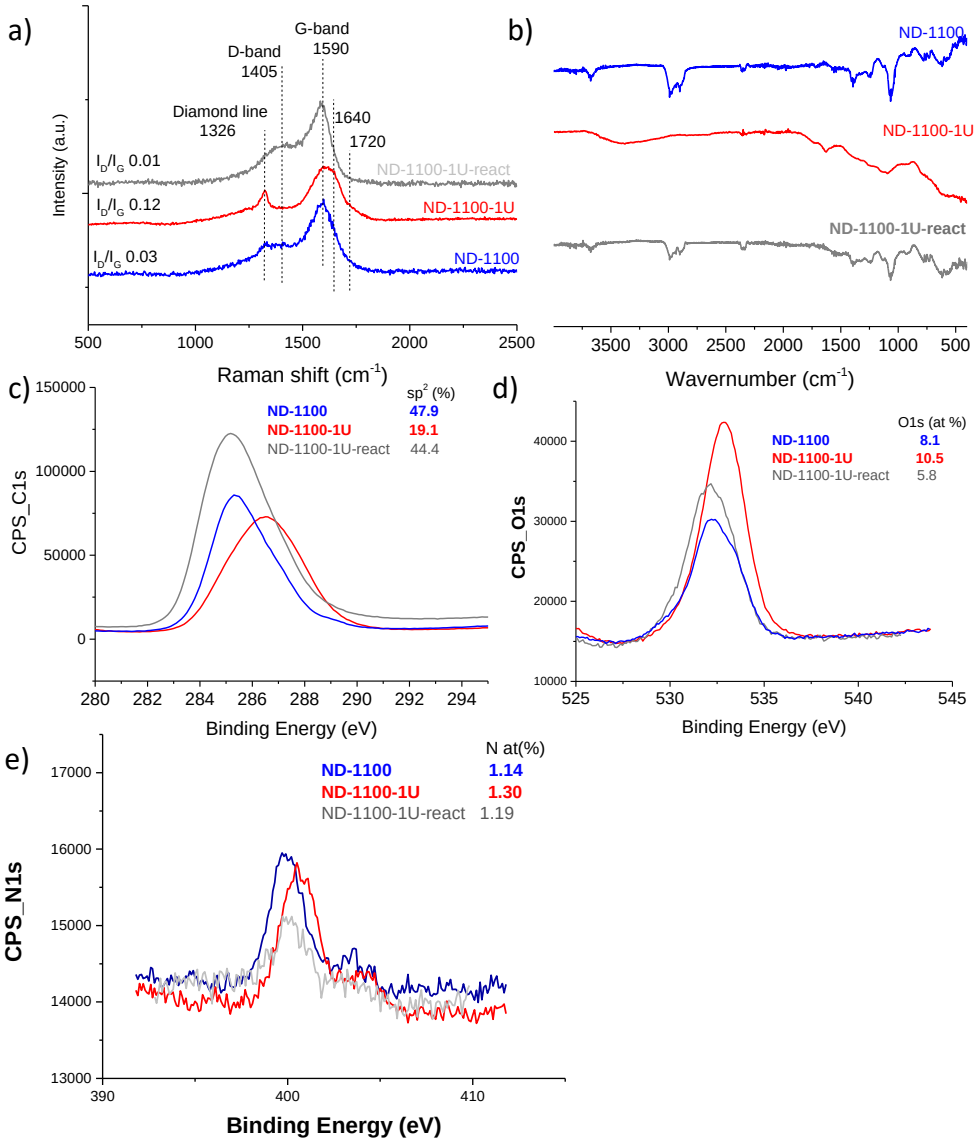

Figure 9. UV-Raman (a), FT-IR (b), XPS C1s (c), XPS O1s (d) and XPS N1s (e) of the fresh (blue line), used (red line), and reactivated (grey line) ND-1100 sample.

EPR spectroscopy has also been employed to investigate the deactivation-activation process of the ND-1100 sample (Figure 10). For the sake of comparison, the commercial ND sample was also measured. Previous studies have shown that the EPR signal of the NDs can be attributed to the presence of carbon dangling bonds with unpaired electrons in the outer part of the ND samples [30, 60]. In our case, the decrease in EPR signal intensity in the ND-1100 samples in comparison with the fresh commercial

ND is attributable to the decomposition and reconstruction of the outer part of the NDs leading to the formation of a graphitic shell with a reduced number of dangling bonds. Partial oxidation of the used ND-1100-1U sample after one catalytic cycle exhibits a more intense EPR signal than the fresh ND-1100 sample. Importantly, the reactivated ND-1100-1U-react sample exhibits an EPR spectrum that is remarkably like that of the fresh ND-1100 sample. These observations can be interpreted considering that the surface of the ND-1100 sample is oxidised during the catalytic ozonation with the corresponding formation of dangling bonds – while a subsequent thermal annealing at 1100 ºC for 1 h reconstitutes the graphitic shell present in the fresh ND-1100 sample.

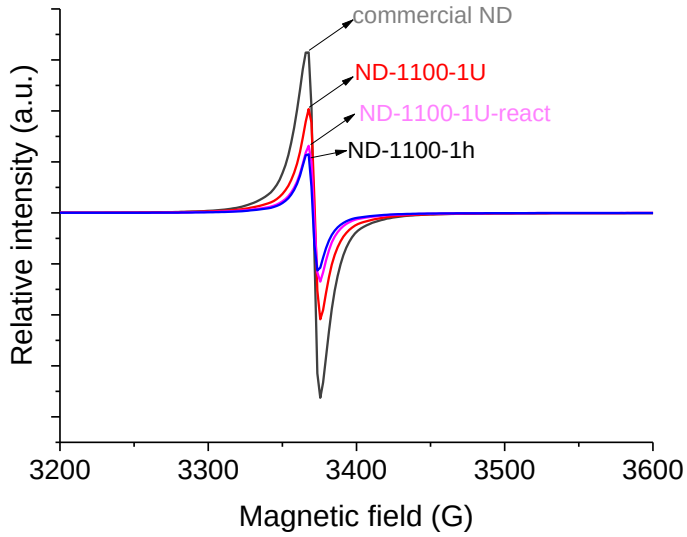

Figure 10. EPR spectra of commercial ND (grey line), ND-1100-1h (blue line), ND-1100 after one catalytic use (ND-1100-1U, red line) and ND-1100 after one catalytic use and reactivated at 1100 ºC for 1 h (ND-1100-1U-react, pink line).

Overall, this section has provided some insights about the nature of the active centres present in the defective and hybrid sp^2/sp^3 nanodiamonds, their transformation during the catalytic ozonation as well as the possibility to restore in large extent the initial structure and catalytic activity.

3.4. ROS during the carbocatalytic ozonation

The nature of the ROS generated during the ozonation process using ND-1100-1h as a metal-free catalyst was addressed using EPR spectroscopy and selective quenching experiments. The use of DMPO and TEMP as spin traps enables the identification of hydroperoxyl and $^1O_2$ species [45], respectively (Figure 11). The formation of $^1O_2$ during the catalytic ozonation of oxalic acid in the presence of ND-1100 as a catalyst at pH 3 was further confirmed by observing that the presence of NaN_3, a selective $^1O_2$ queening agent, largely inhibits the oxalic degradation (Figure S19). In contrast, the presence of DMSO or *tert*-butanol during the catalytic ozonation of oxalic acid does not stop the reaction (data not shown) and this is interpreted as an indirect probe of the absence of hydroxyl radicals during the catalytic process. Attempts to degrade acetic acid, a hydroxyl radical probe molecule during ozonation [61], by catalytic ozonation in the presence of ND-1100 at pH 3 resulted in the absence of catalytic activity. In this case, an adsorption of acetic acid on ND-1100 was about 4 wt%. The generation of hydroperoxyl radicals and $^1O_2$ and the absence of hydroxyl radicals during the carbocatalytic ozonation using ND-1100 is similar to that found when using analogous carbon-based materials such as edge-hydroxylated graphitic carbon [45] or rGO as a ozonation catalysts [46]. These observations could be interpreted considering the occurrence of an electron transfer process from the electron rich hybrid ND-1100 to ozone. However attempts to detect radical species arising from this proposed electron transfer by recording the EPR spectra of a frozen aqueous suspension of ND-1100 submitted to an ozone flow met with failure. After electron transfer, $O_3^{\cdot-}$ would undergo a prompt decomposition to ROS without any chance to record the EPR spectrum of these transient species. In any case, further studies are required to obtain some direct experimental evidence of this electron transfer process from ND-1100 to O_3.[22, 58] Furthermore, TOC measurements of oxalic acid as organic

aqueous pollutant before and after the carbocatalytic ozonation using ND-1100 confirm its complete mineralization to CO_2 and H_2O. The formation of some possible reaction intermediates such as formic acid during the catalytic ozonation of oxalic acid was not observed [62].

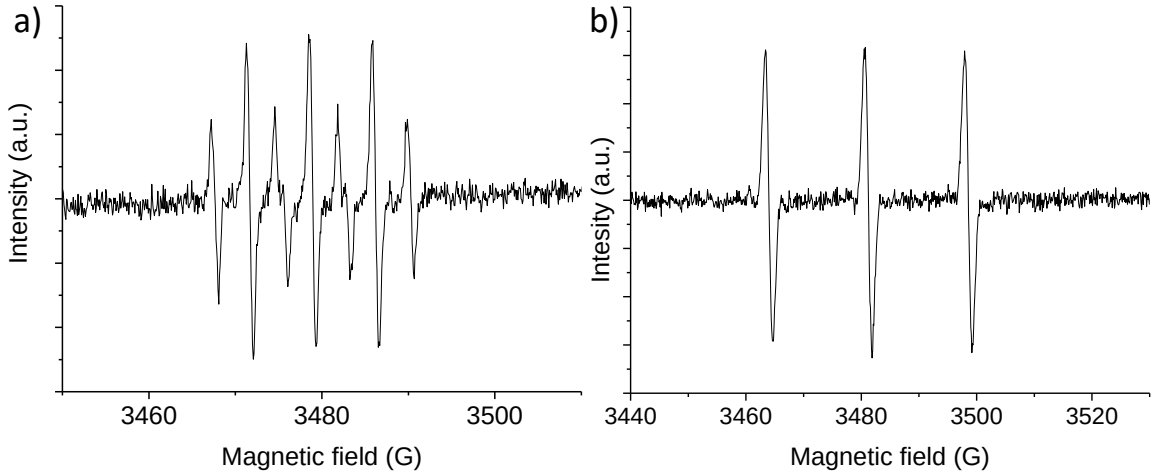

Figure 11. EPR spectra obtained during the ozonation process using ND-1100-1h as a metal-free catalyst in the presence of DMPO (a) or TEMP (b) as trapping agents. Reaction conditions: catalyst (100 mg L^{-1}), O_3 inlet to the glass reactor (140 mg/h), trapping agent (1 g L^{-1}), pH 3, room temperature, and 30 min reaction.

Conclusions

The present study shows that thermally annealing commercial NDs in an inert atmosphere results in the formation of defective hybrid sp^2/p^3 nanodiamonds that perform well as metal-free ozonation catalysts. Characterisation data from PXRD, spectroscopic techniques (UV-Raman, FT-IR, XPS and EPR) and TEM measurements reveal that the thermal annealing of commercial NDs produces a diamond core and graphitic shell together with oxygen and nitrogen functional groups. The higher the annealing temperature of commercial NDs, the greater the graphitic shell, and the lower the density of structural defects. Importantly, a volcano-type trend relationship between the catalytic

activity for oxalic acid degradation and the sp^2/sp^3 ratio of NDs was found. A synergistic effect between the sp^2/sp^3 configuration and the presence of oxygen and nitrogen functional groups for the most active ND-1100 sample was found. It is proposed that the sp^3 core of the ND increases the charge transfer to the graphitic shell while the presence of oxygen functional groups such as hydroxyl, increases the work function of the material and this produces a superior metal-free ozonation catalyst. The activity of the partially spent catalyst can be recovered by a simple thermal annealing process in an insert atmosphere at 1100 ºC. EPR spectroscopy and selective quenching experiments have revealed that hydroperoxyl radicals and $^1O_2$ are the main ROS generated during the catalytic process.

This study has shown the possibility of tailoring the physico-chemical properties of commercial NDs to develop highly active metal-free ozonation catalysts. We are confident that this work will further contribute to expanding the field of metal-free heterogeneous catalysis.

Acknowledgements

E.M.L acknowledges the Generalitat Valenciana for a PhD grant (ACIF/2020/267). S. N. thanks financial support by Ministerio de Ciencia, Innovatión y Universidades RTI2018–099482-A-I00 project and Agència Valenciana de la Innovació (AVI, INNEST/2020/111) project.

References

[1] X. Duan, H. Sun, S. Wang, Metal-free carbocatalysis in advanced oxidation reactions, Acc. Chem. Res., 51 (2018) 678-687.

[2] X.-K. Kong, C.-L. Chen, Q.-W. Chen, Doped graphene for metal-free catalysis, Chem. Soc. Rev., 43 (2014) 2841-2857.

[3] X. Liu, L. Dai, Carbon-based metal-free catalysts, Nat. Rev. Mater., 1 (2016) 16064.

[4] D.W. Stephan, Catalysis, FLPs, and Beyond, Chem. Mater., 6 (2020) 1520-1526.

[5] D.S. Su, S. Perathoner, G. Centi, Nanocarbons for the development of advanced catalysts, Chem. Rev., 113 (2013) 5782−5816.

[6] Y. Wang, X. Wang, M. Antonietti, Polymeric graphitic carbon nitride as a heterogeneous organocatalyst: From photochemistry to multipurpose catalysis to sustainable chemistry, Angew. Chem. Int. Ed., 51 (2012) 68-89.

[7] B. Daelemans, N. Bilbao, W. Dehaen, S. De Feyter, Carbocatalysis with pristine graphite: on-surface nanochemistry assists solution-based catalysis, Chem. Soc. Rev., 50 (2021) 2280-2296.

[8] L. Liu, Y.-P. Zhu, M. Su, Z.-Y. Yuan, Metal-free carbonaceous materials as promising heterogeneous catalysts, ChemCatChem, (2015) 2765-2787.

[9] D.S. Su, G. Wen, S. Wu, F. Peng, R. Schlögl, Carbocatalysis in liquid-phase reactions, Angew. Chem. Int. Ed., 56 (2017) 936-964.

[10] D.R. Dreyer, C.W. Bielawski, Carbocatalysis: Heterogeneous carbons finding utility in synthetic chemistry, Chem. Sci., 2 (2011) 1233-1240.

[11] S. Navalón, W.-J. Ong, X. Duan, Sustainable catalytic processes driven by graphene-based materials, Processes, 8 (2020) 672.

[12] M.-M. Titirici, R.J. White, N. Brun, V.L. Vitaliy L. Budarin, D.S. Dang Sheng Su, F. del Monte, J.H. Clark, M.J. MacLachlan, Sustainable carbon materials Chem. Soc. Rev., 44 (2015) 250-290.

[13] J.C. Espinosa, S. Navalon, M. Alvaro, A. Dhakshinamoorthy, H. Garcia, Reduction of C=C double bonds by hydrazine using active carbons as metal-free catalysts ACS Sustain. Chem. Enginee., 6 (2018) 5607-5614

[14] A. Schraut, G. Zmiga, H.-G. Sockel, Composition and structure of active coke in the oxydehydrogenation of ethylbenzene, Appl. Catal. , 29 (1987) 311-326.

[15] E.H.L. Falcao, F. Wudl, Carbon allotropes: Beyond graphite and diamond, J. Chem. Technol. Biotech., 82 (2007) 524-531.

[16] S. Navalon, A. Dhakshinamoorthy, M. Alvaro, M. Antonietti, H. García, Active sites on graphene-based materials as metal-free catalysts, Chem. Soc. Rev., 46 (2017) 4501-4529

[17] S. Navalon, A. Dhakshinamoorthy, M. Alvaro, H. Garcia, Carbocatalysis by graphene-based materials, Chem. Rev., 12 (2014) 6179-6212.

[18] S. Navalón, J.R. Herance, M. Álvaro, H. García, General aspects in the use of graphenes in catalysis, Mater. Horizons, 5 (2018) 363-378

[19] D.R. Dreyer, A.D. Todd, C.W. Bielawski, Harnessing the chemistry of graphene oxide, Chem. Soc. Rev., 43 (2014) 5288-5301.

[20] H. Hu, J.H. Xin, H. Hu, X. Wang, Y. Kong, Metal-free graphene-based catalyst-insight into the catalytic activity: A short review, Appl. Catal. A.-Gen, 492 (2015) 1-9.

[21] S. Navalón, A. Dhakshinamoorthy, M. lvaro, H. García, Diamond nanoparticles in heterogeneous catalysis, Chem. Mater., 32 (2020) 4116-4143.

[22] X. Duan, W. Tian, H. Zhang, H. Sun, Z. Aoc, Z. Shao, S. Wang, sp2/sp3 framework from diamond nanocrystals: A key bridge of carbonaceous structure to carbocatalysis, ACS Catal., 8 (2019) 7494-7519.

[23] A. Krueger, Beyond the shine: recent progress in applications of nanodiamond, J. Mater. Chem., 21 (2011) 12571–12578.

[24] A. Krueger, D. Lang, Functionality is key: recent progress in the surface modification of nanodiamond, Adv. Func. Mater., 22 (2012) 890-906

[25] G. Filippini, M. Prato, C. Rosso, Carbon dots as nano-organocatalysts for synthetic applications, ACS Catal., 10 (2020) 8090-8105.

[26] Y. Lin, X. Sun, D.S. Su, G. Centi, S. Perathoner, Catalysis by hybrid sp2/sp3 nanodiamonds and their role in the design of advanced nanocarbon materials, Chem. Soc. Rev., 47 (2018) 8438-8473

[27] M. Zeiger, N. Jäckel, V.N. Mochalin, V. Presser, Review: carbon onions for electrochemical energy storage, J. Mater. Chem. A, 4 (2016) 3172-3196.

[28] J. Zhang, D.S. Sheng Su, R. Blume, R. Schlögl, R. Wang, X. Yang, A. Gajovic, Surface chemistry and catalytic reactivity of a nanodiamond in the steam-free dehydrogenation of ethylbenzene, Angew. Chem. Int. Ed., 49 (2010) 8640 -8644.

[29] R. Wang, X. Sun, B. Zhang, X. Sun, D. Su, Hybrid nanocarbon as a catalyst for direct dehydrogenation of propane: formation of an active and selective core–shell sp2/sp3 nanocomposite structure, Chem. Eur. J., 20 (2014) 6324 - 6331.

[30] X. Duan, Z. Ao, H. Zhang, M. Saunders, H. Sun, Z. Shao, S. Wang, Nanodiamonds in sp2/sp3 configuration for radical to nonradical oxidation: Core-shell layer dependence, Appl. Catal. B. Environ., 222 (2018) 176-181.

[31] X.G. Duan, C. Su, L. Zhou, H.Q. Sun, A. Suvorova, T. Odedairo, Z.H. Zhu, Z.P. Shao, S.B. Wang, Surface controlled generation of reactive radicals from persulfate by carbocatalysis on nanodiamonds, Appl. Catal. B. Environ., (2016) 7−15.

[32] X.G. Duan, Z.M. Ao, L. Zhou, H.Q. Sun, G.X. Wang, S.B. Wang, Occurrence of radical and nonradical pathways from carbocatalysts for aqueous and nonaqueous catalytic oxidation, Appl. Catal. B. Environ., 188 (2016) 98−105.

[33] B. Kasprzyk-Hordern, M. Ziółek, J. Nawrocki, Catalytic ozonation and methods of enhancing molecular ozone reactions in water treatment, Appl. Catal. B Environ., (2003) 639-669.

[34] J. Nawrocki, B. Kasprzyk-Hordern, The efficiency and mechanisms of catalytic ozonation, Appl. Catal. B-Environ, 99 (2010) 27-42.

[35] L. Niu, T. Wei, Q. Li, G. Zhang, G. Xian, Z. Long, Z. Ren, Ce-based catalysts used in advanced oxidation processes for organic wastewater treatment: A review, J. Environ. Sci., 96 (2020) 109-116.

[36] P.M. Alvárez, F.J. Beltrán, F.J. Masa, J.P. Pocostales, A comparison between catalytic ozonation and activated carbon adsorption/ozone-regeneration processes for wastewater treatment., Appl. Catal., B, 92 (2009) 393−400.

[37] P.M. Alvarez, J.F. García-Araya, F.J. Beltrán, I. Giráldez, J. Jaramillo, V. Gomez-Serrano, The influence of various factors on aqueous ozone decomposition by granular activated carbons and the development of a mechanistic approach. , Carbon 44 (2006) 3102−3112.

[38] P.C.C. Faria, J.J.M. Orfao, M.F.R. Pereira, Catalytic ozonation of sulfonated aromatic compounds in the presence of activated carbon. , Appl. Catal., B 83 (2008) 150−159.

[39] P.C.C. Faria, J.J.M. Órfão, M.F.R. Pereira, Ozone decomposition in water catalysed by activated carbon: influence of chemical and textural properties, Ind. Eng. Chem. Res., 45 (2006) 2715−2721.

[40] A.G. Gonçalves, J.J.M. Órfão, M.F.R. Pereira, Catalytic ozonation of sulphamethoxazole in the presence of carbon materials, J. Hazard. Mater., 239−240 (2012) 167−174.

[41] M. Sánchez-Polo, U. von Gunten, J. Rivera-Utrilla, Efficiency of activated carbon to transform ozone into OH radicals: Influence of operational parameters. , Water Res. , 39 (2005) 3189−3198.

[42] O.S.G.P. Soares, P.C.C. Faria, J.J.M. Órfão, M.F.R. Pereira, Ozonation of textile effluents and dye solutions in the presence of activated carbon under continuous operation. , Sep. Sci. Technol. 2007, 42 (2007) 1477−1492.

[43] Y.-C. Lin, C.-L. Chang, T.-S. Lin, H. Bai, M.-G. Yan, F.-. Ko, C.-T. H.; Wu, C.-H. Huang, Application of physical vapor deposition process to modify activated carbon fibers for ozone reduction, Korean J. Chem. Eng. , 25 (2008) 446−450.

[44] A.G. Gonçalves, J.L. Figueiredo, J.J.M. Orfao, M.F.R. Pereira, Influence of the surface chemistry of multi-walled carbon nanotubes on their activity as ozonation catalysts, Carbon 48 (2010) 4369−4381.

[45] F. Bernat-Quesada, J.C. Espinosa, V. Barbera, M. Álvaro, M. Galimberti, S. Navalon, H. García, Catalytic Ozonation Using Edge-Hydroxylated Graphite-Based Materials, ACS Sustainable Chem. Eng., 7 (2019) 17443−17452.

[46] Y. Wang, Y. Xie, H. Sun, J. Xiao, H. Cao, S. Wang, Efficient catalytic ozonation over reduced graphene oxide for p-hydroxylbenzoic acid (PHBA) destruction: Active site and mechanism. , ACS Appl. Mater. Interfaces, 8 (2016) 9710−9720.

[47] Y. Wang, X. Duan, Y. Xie, H. Sun, S. Wang, Nanocarbon-based catalytic ozonation for aqueous oxidation: Engineering defects for active sites and tunable reaction pathways, ACS Catal., 10 (2020) 13383–13414.

[48] F.J. Beltran, F.J. Rivas, R. Montero-de-Espinosa, Ozone-enhanced oxidation of oxalic acid in water with cobalt catalysts. 1.Homogeneous catalytic ozonation., Ind. Eng. Chem. Res. , 42 (2003) 3210−3217.

[49] D.S. Pines, D.A. Reckhow, Effect of dissolved cobalt(II) on the ozonation of oxalic acid. , Environ. Sci. Technol., 36 (2002) 4046−4051.

[50] J. Gomes, R. Costa, R.M. Quinta-Ferreira, R.C. Martins, Application of ozonation for pharmaceuticals and personal care products removal from water, Sci. Total Environ., 586 (2017) 265-283.

[51] J. Ackermann, A. Krueger, Efficient surface functionalization of detonation nanodiamond using ozone under ambient conditions, Nanoscale, 11 (2019) 8012-8019.

[52] V. Mochalin, S. Osswald, Y. Gogotsi, Contribution of functional groups to the Raman spectrum of nanodiamond powders, Chem. Mater., 21 (2009) 273–279.

[53] T. Ando, K. Yamamoto, M. Ishii, M. Kamo, Y. Sato, Vapour-phase oxidation of diamond surfaces in O2 studied by diffuse reflectance Fourier-transform infrared and temperature-programmed desorption spectroscopy, J. Chem. Soc. Trans. Faraday, 89 (1993) 3635-3640.

[54] Y. Cao, X. Luo, H. Yu, F. Peng, H. Wang, G. Ning, sp2- and sp3-hybridized carbon materials as catalysts for aerobic oxidation of cyclohexane, Catal. Sci. Technol., 3 (2013) 2654-2660.

[55] J.C. Espinosa, S. Navalón, A. Primo, M. Moral, J. Fernández Sanz, M. Álvaro, H. García, Graphenes as efficient metal-free Fenton catalysts, Chem. Eur. J., 21 (2015) 11966–11971.

[56] J.C. Espinosa, S. Navalón, M. Álvaro, H. García, Reduced graphene oxide as a metal-free catalyst for the light-assisted Fenton-like reaction, ChemCatChem, 8 (2016) 2642-2648.

[57] X. Duan, H. Sun, Z. Ao, L. Zhou, G. Wang, S. Wang, Unveiling the active sites of graphene-catalyzed peroxymonosulfate activation, Carbon, 107 (2016) 371-378.

[58] Y. Wang, N. Ren, J. Xi, Y. Liu, T. Kong, C. Chen, Y. Xie, X. Duan, S. Wang, Mechanistic investigations of the pyridinic N−Co structures in Co embedded N-doped carbon nanotubes for catalytic ozonation, ACS EST Engg. , 1 (2021) 32−45.

[59] J. Xiao, Q. Han, Y. Xie, J. Yang, Q. Su, Y. Chen, H. Cao, Is C3N4 chemically stable toward reactive oxygen species in sunlight driven water treatment? , Environ. Sci. Technol., 51 (2017) 13380−13387.

[60] A.A. Soltamova, I.V. Ilyin, P.G. Baranov, A.Y. Vul', S.V. Kidalov, F.M. Shakhov, G.V. Mamin, S.B. Orlinskii, N.I. Silkin, M.K. Salakhov, Detection and identification of nitrogen defects in nanodiamond as studied by EPR, Physica. B, 404 (2009) 4518-4521.

[61] T. Shen, Q. Wang, S. Tong, Solid Base MgO/Ceramic honeycomb catalytic ozonation of acetic acid in water, Ind. Eng. Chem. Res., 56 (2017) 10965−10971.

[62] Y. AlSalka, A. Hakki, M. Fleisch, D.W. Bahnemann, Understanding the degradation pathways of oxalic acid in different photocatalytic systems: Towards simultaneous photocatalytic hydrogen evolution, J. Photoch. Photobio. A., 366 (2018) 81-90.